European Journal of Radiology 112 (2019) 93–105

Contents lists available at ScienceDirect

European Journal of Radiology

journal homepage: www.elsevier.com/locate/ejrad

Review

High resolution MRI of nail tumors and tumor-like conditions

Pravin Mundada[a], Minerva Becker[a], Vincent Lenoir[a], Salvatore Stefanelli[a], Anne-Laure Rougemont[b], Jean Yves Beaulieu[c], Sana Boudabbous[a,*]

[a] Division of Radiology, Department of Imaging and Medical Informatics, Geneva University Hospitals, University of Geneva, Rue Gabrielle-Perret-Gentil 4, 1211, Geneva 14, Switzerland
[b] Division of Clinical Pathology, Department of Genetic and Laboratory Medicine, Geneva University Hospitals, University of Geneva, Rue Gabrielle-Perret-Gentil 4, 1211, Geneva 14, Switzerland
[c] Division of Hand Surgery, Department of Orthopedic Surgery, Geneva University Hospitals, University of Geneva, Rue Gabrielle-Perret-Gentil 4, 1211, Geneva 14, Switzerland

ARTICLE INFO

Keywords:
Nail
Benign tumors
Malignant tumors
Magnetic resonance imaging (MRI)

ABSTRACT

Although the nail is a small anatomical structure, it can be affected by various tumors and tumor-like conditions. Because of the distinctive nail anatomy, the clinical presentation of tumors is modified, thus rendering the diagnosis challenging. As nail biopsy and surgery are painful procedures associated with an increased risk of permanent onychodystrophy, pre-operative diagnosis is desirable. Although conventional radiographs are still the first-line radiologic examination for the assessment of bony structures beneath the nail matrix, they do not allow detailed evaluation of the phalangeal soft tissues. High resolution MRI allows accurate detection and mapping of nail lesions and can suggest a specific diagnosis. This review focuses on high resolution MRI of nail tumors and tumor-like lesions. We review the nail anatomy and the optimal MRI protocol. We then discuss a variety of tumors and tumor-like lesions in relation to the clinical presentation, anatomic location, histological features and imaging characteristics. We herewith describe common benign tumors (glomus tumor, onychomatricoma, keratoakanthoma, fibroma, subungual exostosis, hemangioma, chondroma, pyogenic granuloma), malignant tumors (subungual melanoma, subungual squamous cell carcinoma), as well as tumor mimics (mucoid cyst, epidermoid cyst). Although not entirely specific, MRI is a valuable tool in treatment planning of these tumors.

1. Introduction

Finger and toe nails are anatomically complex skin appendages that provide protection to finger and toe tips and contribute to the versatility of finger and toe functions including proprioception, scratching and picking [1]. Nail apparatus disorders can occur following trauma with or without foreign body penetration, infection and thermal injuries or in the context of systemic conditions, such as iron deficiency anemia, sarcoidosis, psoriasis and collagen disorders. Although rare, tumors and tumor-like conditions can equally involve the nail apparatus [2]. As the nail plate tends to modify the appearance and growth of subungual and periungual tumors, the clinical appearance of nail tumors may be nonspecific, for eg. a lesion arising beneath the proximal nail fold may manifest clinically only as a longitudinal nail groove. Other non-specific features include nail discoloration, pain and nail deformity. Due to their nonspecific clinical appearance but functional importance, early detection, precise depiction of tumor spread and lesion characterization play an important role for treatment planning. Glomus tumor, fibroma, subungual exostosis, kerathoacanthoma, onychomatricoma, hemangioma and mucoid cyst are the most common benign lesions, whereas the most common malignant neoplasms include squamous cell carcinoma (SCC), malignant melanoma and metastasis [3–5]. Cancers that tend to metastasize to the nail apparatus include lung, genitourinary and breast cancers [2].

The small size of the fingers and toes renders imaging of the nail unit challenging. Conventional radiographs can detect calcifications and gross adjacent bone invasion. Although ultrasonography (US) performed with a high-frequency transducer can effectively depict tumors, their small size, flattened shape, artifacts and operator experience limit tissue characterization. Due to continuous advances in MRI

* Corresponding author.
E-mail addresses: mundada.pravin@gmail.com (P. Mundada), Minerva.Becker@hcuge.ch (M. Becker), Vincent.Lenoir@hcuge.ch (V. Lenoir), Savlatore.Stefanelli@hcuge.ch (S. Stefanelli), Anne-Laure.Rougemont@hcuge.ch (A.-L. Rougemont), jeanyves.beaulieu@hcuge.ch (J.Y. Beaulieu), Sana.Boudabbous@hcuge.ch (S. Boudabbous).

https://doi.org/10.1016/j.ejrad.2019.01.004
Received 17 August 2018; Received in revised form 30 October 2018; Accepted 4 January 2019
0720-048X/ Published by Elsevier B.V.

technology, high-resolution imaging of the nail apparatus is feasible today in clinical routine. It can be used as a problem-solving tool in unclear or equivocal cases. MRI provides an accurate and detailed analysis of the nail apparatus and allows detection and correct depiction of nail tumors, in particular, evaluation of their relationship with adjacent structures, thus contributing to an improved pre-therapeutic planning. However, to the best of our knowledge only very few publications have so far dealt with MRI of nail apparatus tumors. Furthermore, most publications on the topic are based on imaging at 1.5 T. At 3 T, the higher signal to noise ratio allows obtaining images with higher resolution than at 1.5 T. Further advantages at 3 T include faster imaging and the routine use of 3D sequences with very high temporal (sub-second) resolution and highest anatomic detail due to sub-millimeter spatial resolution, all of which are essential for the depiction of subtle abnormalities of the nail apparatus and for the detection of small vascular tumors. The purpose of the current article is to provide an understanding of the MRI-relevant nail anatomy, to discuss the routine high-resolution MR imaging protocol at 3 T, to illustrate a variety of nail tumors and to understand the limitations of MRI regarding tumor characterization.

2. Gross anatomy and MRI appearance of the normal nail apparatus

Understanding the anatomy of the nail unit is necessary for the diagnosis of nail tumors, for biopsy planning and for surgical management. The nail apparatus comprises a nail plate (commonly referred to as “the nail”), proximal and lateral nail folds, a nail matrix and a nail bed (Fig. 1). The distal phalanx and the distal interphalangeal joint along with the synovium, ligaments, and the extensor tendon insertion are also part of the nail apparatus [6]. The nomenclature used for describing the various parts of the nail apparatus varies in the literature. We have attempted to acquaint the readers with these terminologies.

The nail plate (nail) is an opalescent sheet of compacted keratinized cells, which grows throughout life. The nail plate shows a “tram-track” appearance on high-frequency ultrasound [7], and it appears as a single homogeneously hypointense plate on MRI (Fig. 1). The lateral nail folds (LNF, paronychium) are cutaneous folds on the sides of the nail that hold the nail plate in place and provide lateral borders. The proximal nail fold (PNF) is a cutaneous fold that covers the proximal part of the nail plate. Its dorsal surface is a continuation of the adjacent skin. Its free edge continues as cuticle (eponychium) which is adherent to the dorsal surface of the proximal nail plate and provides a protective seal. The nail matrix is a highly proliferative epithelial structure that forms a nail-producing cul-de-sac around the root of the nail plate. The ventral aspect of the PNF forms the dorsal part of the matricial cul-de-sac that is referred to as the dorsal matrix (also described as proximal matrix by few authors). The dorsal matrix produces a thin cell layer along the dorsal aspect of the nail plate that imparts the shiny appearance to the nail. The ventral floor of the matricidal cul-de-sac forms the ventral nail matrix (germinal matrix, distal matrix, intermediate matrix) that produces the major part of the nail plate. The ventral matrix has lateral horn-like extensions on either side. The ventral matrix transitions distally to continue as the nail bed (sterile matrix). The ventral surface of the nail plate firmly adheres to the nail bed. The nail bed occasionally contributes to the formation of the ventral aspect of the nail plate. The nail bed extends distally till the hyponychium. The lunula is a half-moon shaped area at the base of the nail plate that appears paler than the distal part of the nail and has a distal convex margin. It is generally visible on the thumbs and great toe. Sometimes, the lunula is completely concealed by the proximal nail fold. In 1996, Drape et al. demonstrated that the lunula corresponds to a distinct oval-shaped area in the sub-matricial dermis, which appears homogeneously hyperintense on T2-weighted images and shows homogeneous enhancement after gadolinium injection [8]. However, in the subsequently published literature, most authors continued to regard the lunula as the topographical representation of the underlying ventral matrix. The rest of the dermis appears predominantly hypointense with few scattered hyperintense foci on T2-weighted images.

Several connective tissue strands directly anchor the dermis on the dorsal periosteum of the distal phalanx. There is no subcutaneous fat layer seen between the dermis and the periosteum. MRI consistently demonstrates a curvilinear hypointense band extending from the proximal end of the ventral matrix to the dorsal aspect of the base of the distal phalanx [8]. This hypointense band most likely corresponds to the laminar extension of the extensor tendon encasing the germinal matrix [9,10]. Histopathological and cadaveric dissection studies have shown the presence of lateral horns of the ventral matrix and various ligamentous anchoring of the ventral matrix. These structures are not discernible on MRI. The cutaneous margin underlying the free nail is the hyponychium, which is bordered distally by the distal groove. The distal groove (limiting furrow) is the cutaneous ridge demarcating the border between subungual structures and the finger pulp. The onychodermal band is the distal margin of the nail bed with a contrasting hue in comparison with the rest of the nail bed.

3. The role of imaging in nail tumors

Despite their superficial location, tumors of the nail apparatus often pose a diagnostic dilemma. Imaging thus helps in the diagnosis and localization of the tumor. Identification of the correct location and tumor extent can contribute to determining the surgical approach. Despite its limited value, plain radiography is the first and most commonly requested imaging modality for the evaluation of a suspected nail tumor. It is useful for the diagnosis and follow-up of subungual exostosis and it can detect soft tissue calcifications. In one series of 44 glomus tumors of nail beds, plain radiographs identified bone erosion in 25% of cases [11]. In another series of glomus tumors of the nail bed, comparative lateral radiographs of hands showed increased distance between the dorsal aspect of the phalanx and the nail in 25% of cases [12]. Plain radiographs in cases of subungual carcinoma may show no radiographic evidence of bony involvement even though the periosteum may be invaded by tumor. Similarly, some authors have shown that in cases in which the subungual SCC was microscopically limited to the soft tissues of the finger, patients may still show radiographic bone changes falsely suggesting invasion [13].

Lack of soft tissue resolution limits the utility of CT for the evaluation of nail tumors. However, CT can readily detect the nidus of osteoid osteomas, soft tissue calcifications and bone erosions.

High-resolution ultrasonography (US) is an accessible and a cost-effective imaging modality. A high-resolution ultrasound performed with color Doppler depicts the fine anatomical details of the nail apparatus. In experienced hands, it reliably detects small benign tumors and tumor-like conditions of the nail apparatus and delineates their anatomical context and vascularity [14,15]. Tissue characterization of various nail unit tumors on ultrasound is, however, limited. Additionally, artifacts limit the detection of flat or small nail tumors [5,16,17]. In addition, bone invasion may be missed with US. Therefore, MRI is regarded as a problem-solving tool in unclear cases. Furthermore, although a pilot study demonstrated the ability of high-velocity high-frequency ultrasound to detect small subungual glomus tumors [18], the literature on ultrasound features of non-glomus tumors of the nail unit and of malignant tumors of the nail is very sparse and virtually lacking.

On high resolution 3 T MRI, accurate anatomical assessment of the nail apparatus is routinely possible. MRI can detect tumors and tumor-like lesions as small as 1–2 mm (see paragraph on glomus tumors) and can help in the pre-operative characterization of mucoid cysts, glomus tumors, keratocanthoma, exostosis and onychomatrichoma. Sub-matricial mucoid cysts are not rare and can be detected only on high resolution MRI [19]. Preoperative detection of a communication between subungual or periungual mucoid cyst with the interphalangeal joint

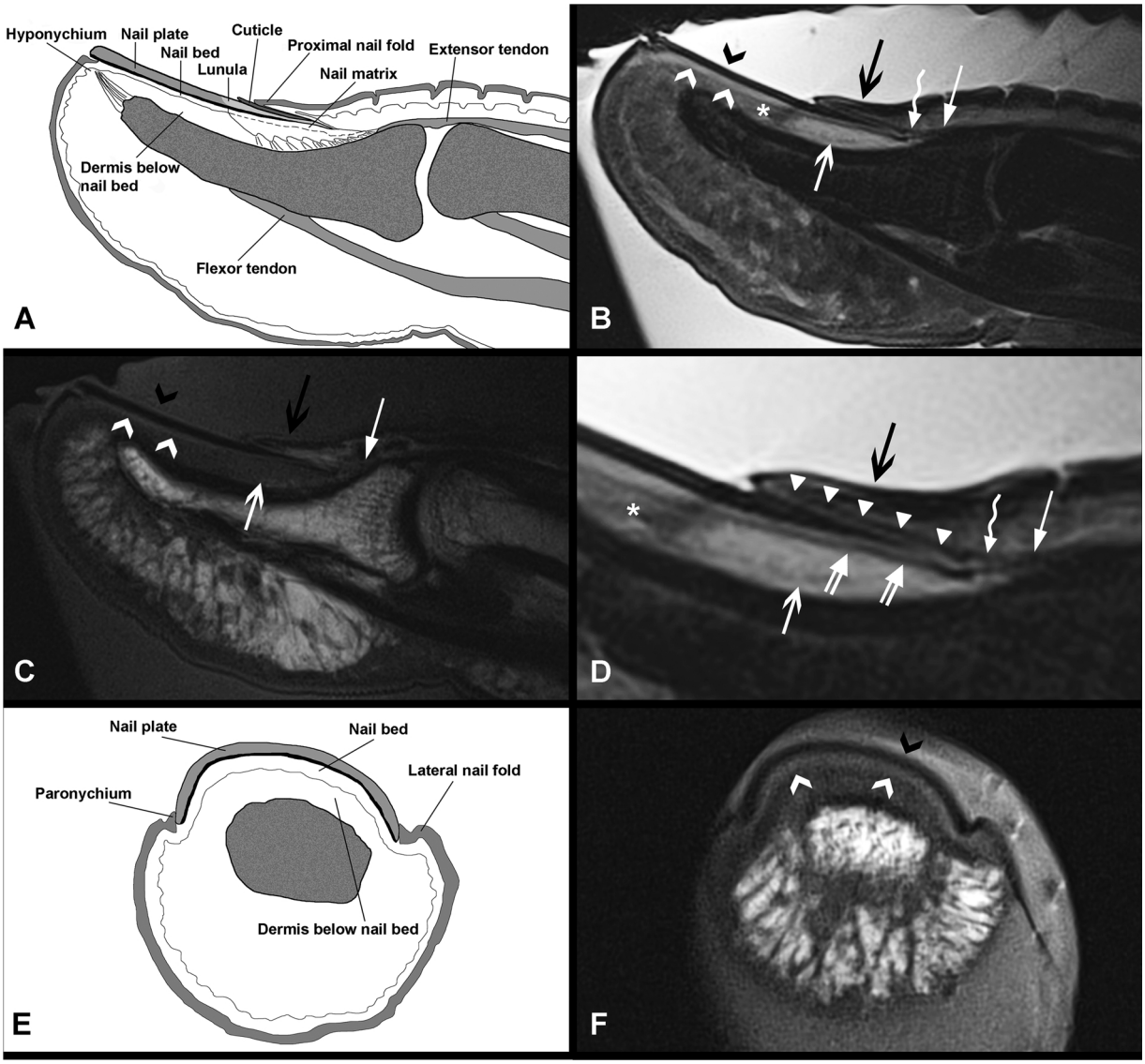

Fig. 1. Normal nail anatomy. Sagittal plane: schematic drawing (A), fat saturated proton density (B and D) and T1-weighted (C) images. Axial plane: schematic drawing (E) and T1-weighted (F) image. Nail plate (B, C and F- black open arrowheads), proximal nail fold, (B, C and D- black open arrows), dorsal matrix (D- white arrowheads), intermediate matrix (D- double arrows), ventral matrix in nail bed (B, C and F- white open arrowheads), extensor tendon (B, C and D- white arrows). The dermis below the nail bed appears homogeneously isointense on the T1-weighted image (C- white open arrow). The proximal part of the dermis shows an oval shaped hyperintense area on proton density images (B and D- white open arrow) and its distal part shows heterogeneous intermediate signal intensity (B and D- asterisk). The thin linear hypointense structures seen posterior to the intermediate matrix (B and D- curved arrows) are thought to be fibrous septae extending from the extensor tendon insertion.

helps the surgical management and prevents cyst recurrence. In the management of squamous cell carcinoma and malignant melanoma, the presence or absence of bone involvement determines the surgical approach. Plain radiographs are known to have a considerable number of false positive or false negative results in detecting early erosion or periosteal infiltration [13]. On the contrary, high resolution MRI is highly sensitive for the detection of early bone invasion [5].

4. MR imaging technique at 3T

MRI of nails is usually performed on a 3 T machine with 4 cm loop flex and phased-array multichannel wrist coils (Fig. 2). In our institution, scans of the fingernails are performed by keeping the patient prone and in hand-first position. The hand is stabilized in full pronation. Scans of the toenail are carried out by keeping the patient supine and in feet-first position (Fig. 2). Our standard protocol includes high-resolution sequences (SE T1-weighted, STIR, proton density with fat saturation), dynamic angiographic 3D acquisitions (TWIST), 3D VIBE and SE T1-weighted sequences with and without fat saturation after iv. gadolinium injection (the exact imaging protocol and the respective sequence parameters are described in Table 1.

Common benign solid tumors involving the nail apparatus include onychomatricoma, subungual keratoacanthoma, subungual and periungual fibroma, glomus tumors and subungual exostosis. Common cystic lesions mimicking tumors clinically comprise epidermoid and mucoid cysts, whereas the most common malignant nail tumors are SCC and melanoma (Table 2).

5. Benign tumors

5.1. Onychomatricoma

Onychomatricoma most commonly occurs in middle age and affects male and females equally. Fingernails are more often involved than

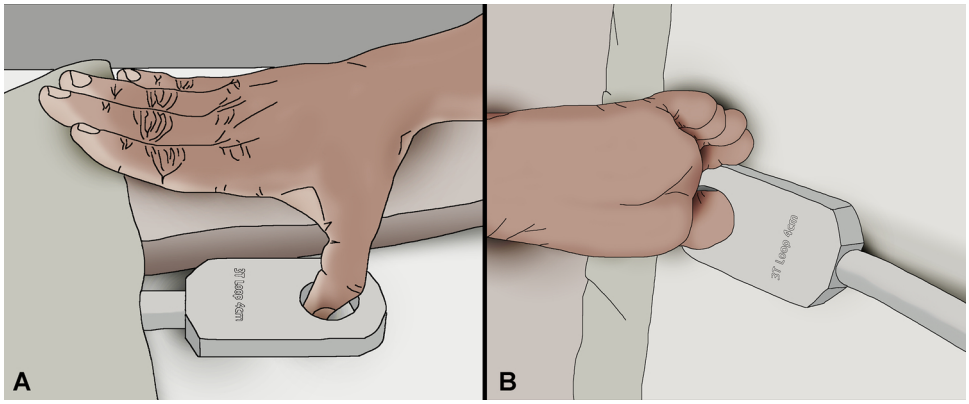

Fig. 2. MRI of fingernails is performed by keeping the patient prone with "hands-first" position (A), whereas MRI of toenails (B) is performed by keeping the patient prone with " feet-first" position. The thumb and toe are held in a special loop flex and phased-array multichannel wrist coil.

toenails. Clinical presentation of these tumors includes slow progressive painless nail dystrophy, yellow discoloration of the nail plate, splinter haemorrhages and, ungula hyperkeratosis [20,21]. Rarely, these tumors may involve more than one nail [22]. Grossly, onychomatricoma is a pedunculated villous tumor. Its characteristic distal digitations extending to the nail plate gives a funnel or Y- shaped appearance to the nail. Most often, these tumors are eccentrically located in the nail and involve one of the matricial horns [14]. Histopathological and imaging correlation is required to differentiate this entity from a rare mimic hypopigmented onychocytic matrichoma [23]. Histopathologically, onychomatricoma is a fibroepithelial tumor with two characteristic distinct zones. The distal zone has `glove–finger` papillary projections and the base has vertically oriented deep invaginations around V-shaped empty cavities [24].

Radiography typically reveals no bony erosion or remodeling. On ultrasound, the tumor appears avascular and predominantly hypoechoic with internal linear hyperechoic areas [14]. High-resolution MRI shows characteristic features (Fig. 3) [25]. On sagittal T2 weighted and proton density images, the tumor appears as a hyperintense well-defined mass with filamentous extension in the thickened funnel-shaped nail plate base. Axial images show tiny holes filled with hyperintense filamentous tumor extensions in the thickened nail plate [4]. The tumor shows homogeneous enhancement after injection of gadolinium. Care must be taken to differentiate the tumor from the oval shaped hyperintense area within the sub-matricial dermis (Fig. 3).

Given the indolent nature of this tumor and no known malignant potential, observation alone may be sufficient in many instances. For symptomatic tumors, tangential excision is preferable to prevent nail deformity, but it involves the risk of incomplete removal. Mohs micrographic surgery (individual tissue layers are removed and examined under the microscope one at a time until all tumor tissue has been removed) allows for clearance of the tumor with minimal removal of the unaffected nail matrix and, thus, minimizes the potential cosmetic and functional impact of surgery [26].

5.2. Subungual keratoacanthoma

Subungual keratoacanthoma (SUKA) is a rare controversial tumor of the nail apparatus with the commonest location being the distal part of the nail bed and, occasionally, arising from the proximal nail fold. It shows a male predilection with peak occurrence in the 5th decade. The exact cause of SUKA is uncertain. Various proposed causative factors include exposure to harsh sunlight, coal tar, chemicals, trauma, burns and clinical conditions like atopic dermatitis, eczema and scleroderma [4,5,27]. It is a rapidly growing, painful and local destructive tumor. Unlike keratoacanthoma occurring elsewhere in the body, spontaneous regression of SUKA is rare [4,5,27]. Interestingly, a rare case of spontaneous regression of SUKA showed re-ossification of the lytic lesion of the phalanx [28].

Grossly, the tumor appears as a red scaly nodule. Histopathologically, keratoacanthoma shows marked acanthosis and epidermal hyperkeratosis with the center filled with keratin. Unlike keratoacanthoma of hairy skin, SUKA lacks the typical epithelial collarette, has less associated inflammation and more dyskeratotic eosinophilic cells. The controversies regarding the histopathological spectrum of SUKA and its overlap with that of ungual SCC are beyond the scope of this article. It is, nevertheless, important to remember that, at times, keratoacanthoma are difficult to differentiate from squamous cell carcinoma (SCC), clinically and histopathologically [28].

On plain radiographs, SUKA shows a well-defined cup-shaped lytic resorption in the distal phalanx, most likely due to pressure erosion, with no surrounding periosteal reaction or sclerosis [29]. A small non-compressive SUKA may present without any bony erosion [30]. On ultrasound, the tumor appears as a non-specific mixed echogenic avascular mass with posterior acoustic enhancement and erosion of the adjacent part of the phalanx [27].

On MRI, SUKA has intermediate signal intensity on T1-weighted and mixed signal intensity mass on T2-weighted images (Fig. 4). Post-gadolinium fat saturated T1 weighted images show thin rim enhancement, which corresponds with inflammatory changes. The central part of the tumor typically shows no enhancement (Fig. 4) [4,5,27].

Most authors find local excision and curettage sufficient and consider these options as the initial treatment of choice. Amputation is reserved when eradicative curettage is difficult or in cases of recurrence [31,32]. Mohs micrographic surgery at the time of curettage may reduce the potential risk of persistent or recurrent tumor and may allow the preservation of the involved fingertip [32].

5.3. Subungual and periungual fibroma

Periungual fibromas also called subungual fibromas or digital fibrokeratomas are painless and slow growing nodules, which can develop in subungual and periungual epidermal structures. Large subungual fibroma appears as a pink nodule lifting the nail plate associated with hyperkeratosis [21,33]. Subungual fibromas most commonly occur in patients with tuberous sclerosis with their incidence being as high as 80% in patients over 30 years of age [21]. The exact cause of subungual fibroma is not known but some authors have shown that mutations in chromosome 9 and 16 appear to occur both in patients with and without tuberous sclerosis while others suggested that subungual fibroma occurring in the non-tuberous sclerosis patient may be caused by previous trauma [34]. Bowen`s disease may mimic fibroma and requires histopathology correlation. Histopathologically, fibroma shows hyperkeratosis, irregular thickening of the epidermis, and interstitial spindle shaped fibrous cells and fibroblasts.

On plain radiography, fibroma may present as soft tissue swelling

Table 1
MRI protocol used in our institution on a 3 T machine with 4 cm loop flex and phased-array multichannel wrist coils (see Fig. 2. for patient positioning).

Sequence	Localizer tra	Localizer cor + sag	Localizer	T1 SE tra	T2 TIRM tra	pd BLADE fs sag	TWIST cor	T1 SE fs tra Gd	T1 SE fs sag Gd	3D T1 VIBE fs tra Gd
Imaging plane	transverse	coronal + sagittal	transverse + coronal + sagittal	transverse	transverse	sagittal	coronal	transverse	sagittal	transverse
Type of sequence	FLASH	FLASH	FLASH	SE	STIR	TSE BLADE	FLASH dyn	SE	SE	FLASH
TR (ms)	15	15	15	450	6230	3000	4.32	567	340	13.9
TE(ms)	5	5	5	19	69	61	1.67	17	17	6.99
Flip angle	40	40	40	90 / 180	90 / 150	90 / 160	25	90 / 180	90 / 180	12
FOV	290	250	150	53	44	56	70	53	53	60
Matrix	256	256	256	384	320	320	128	384	384	320
NEX	1	1	1	1	2	1	1	1	1	1
Parallel imaging factor	none	none	none	none	none	none	none	none	none	none
Phase encoding direction	AP	RL / AP	AP/RL/AP	RL	RL	AP	RL	RL	FH	FH
In plane resolution (mm2)	0.6 × 0.6	0.5 × 0.5	0.3 × 0.3	0.1 × 0.1	0.1 × 0.1	0.2 × 0.2	0.3 × 0.3	0.1 × 0.1	0.1 × 0.1	0.2 × 0.2
Thickness (mm)	8	7	5	2.5	3	2	0.5	2.5	2.5	0.2
Scan time per sequence (min:sec)	0:7.3	00:17	00:19	02:55	04:04	04:17	02:59	03:40	01:48	05:55
Other remarks					TI 180 ms		dyn scan time 3.76 sec, 43 measurements	fs strong	fs strong	fs quick

Abbreviations: AP: antero-posterior, BLADE: PROPELLER sequence (periodically rotated overlapping parallel lines with enhanced reconstruction), cor: coronal, dyn: dynamic, FLASH : Fast Low Angle Shot, FOV: field of view, fs: fat saturation, Gd: gadolinium, mm: millimeter, ms: millisecond, NEX: number of excitations, pd: proton density, RL: right-left, sat: saturation, sag: sagittal, SE: spin echo, sec: second, STIR: Short T1 Inversion Recovery, TE: echo time, TIRM: Turbo Inversion Recovery Magnitude, TR: repetition time, Tra: transverse, TSE: Turbo Spin Echo, TWIST: Time-Resolved Angiography With Interleaved Stochastic Trajectories, VIBE: Volume Interpolated Breathhold Examination.

associated with pressure erosion of bone. On ultrasound, it appears hypovascular. MRI appearance of fibroma varies according to the fibrous content of the tumor. Most often fibroma demonstrates low signal intensity on all sequences (Fig. 5). Sometimes, the presence of mucoid stroma may give a mildly heterogeneous hyperintense appearance on T2-weighted images.

Surgical excision is the most favored treatment option [4]. Alternatively, CO2 laser and phenolization shaving can be performed [21]. Prognosis is excellent.

5.4. Glomus tumor

Of all tumors of the nail apparatus, glomus tumor remains the most extensively discussed tumor in the radiological literature. Glomus tumors account for less than 5% of all hand tumors. Detection of multiple glomus tumors at the time of diagnosis is rare [5]. Location in the hands accounts for about 65–75 % of glomus tumors in the body, and 50–65% of lesions are located at fingertips and toe tips. Digital glomus tumors show female preponderance and present typically between 30–50 years of age [35–37]. Literature reports the association of glomus tumor of hands with Horner's syndrome and neurofibromatosis type 1 [35,38].

Clinical presentation of subungual glomus tumor includes characteristic triad of excruciating paroxysmal pain, tenderness and, sensitivity to cold and mild trauma [35]. However, up to 23% of subungual glomus tumors may not show the typical triad of symptoms [39]. At clinical inspection, ridging and discoloration of the nail are observed. Histopathologically, glomus tumor is a hamartoma of glomus bodies, which show a particularly high concentration in the dermis of the nail bed [24]. Glomus bodies consist of an arteriovenous anastomosis, a neurovascular retinaculum and a smooth muscle component. Glomus tumor arises from hyperplasia of one or more of the elements of glomus body.

Plain radiography features include bone erosion, intra-osseous lytic lesion, and sometimes, only widening of the distance between the nail and bone. On ultrasound, subungual glomus tumors are difficult to evaluate as compared to those in periungual location. The lesion appears as a non-specific hypoechoic solid mass, often associated with erosion of underlying bone. Doppler imaging shows high-velocity flow in the most, but not in all, of the cases [18,40,41].

In most cases, the MRI appearance of glomus tumors resembles that of hemangiomas or other hypervascular lesions. Nevertheless, the MRI aspect varies according to the histological composition. As vascular glomus tumors are composed of numerous vascular lumina, they appear strongly hyperintense on T2-weighted images and MRI angiography shows avid enhancement in the arterial phase, as well as progressive enhancement in the venous phase due to intratumoral shunt vessels (Fig. 6). Solid glomus tumors are composed of epithelioid cells with sparse vascular lumina. They are difficult to detect on MRI because they appear almost isointense to the adjacent dermis on pre- and post-gadolinium sequences. MR angiography is noncontributory due to the paucity of vascular lumina in the tumor. The depiction of a thin hypointense capsule, bone erosion and matrix indentation on thin slice gradient echo 3D images helps in the diagnosis (Fig. 6). Mucoid type of glomus tumor shows mucoid degeneration of stroma, which appears strongly hyperintense on T2-weighted images and shows rim enhancement. It is not rare to see a combination of all three tumor patterns both on histology and MRI.

The role of MRI in subungual glomus tumors is somewhat controversial. In a series of 42 cases with the clinical diagnosis of a glomus tumor of the hand, MRI and subsequent surgery (histology of the surgical specimens: 40 glomus tumors, one neuroma and one skin appendage cystic tumor), Al Qattan et al. found that MRI sensitivity was 90%, specificity was 50%, positive predictive value was 97%, and negative predictive value was 20% [42]. The 4 false negative MRI cases in this study were caused by small (2 mm in diameter) glomus tumors and the lack of delineation of the lesions by MRI was attributed to their small

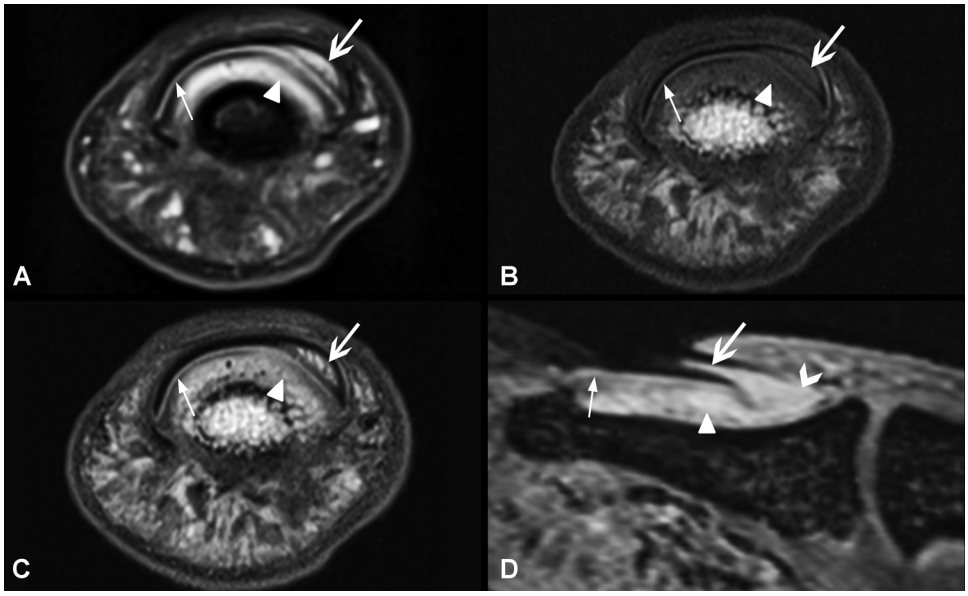

Fig. 3. Onychomatricoma arising from the ventral nail matrix appears hyperintense on fat saturated proton density (A), isointense to dermis on T1 (B) and with enhancement on post contrast T1 weighted images (C and D). The tumor appears as an enhancing mass with Y-shaped extension in the nail plate on the post-contrast 3D VIBE sagittal image (D- open arrowhead). The filamentous extensions of the tumor (D- open arrow) appear as tiny bright holes in the eccentrically thickened nail plate on axial fat saturated proton density and on post-contrast T1 weighted images (A, B and C - open arrows). The enhancing zones in the nail bed (thin arrows) and in the sub-matricial dermis (triangular arrowheads) should not be confused with tumor extension.

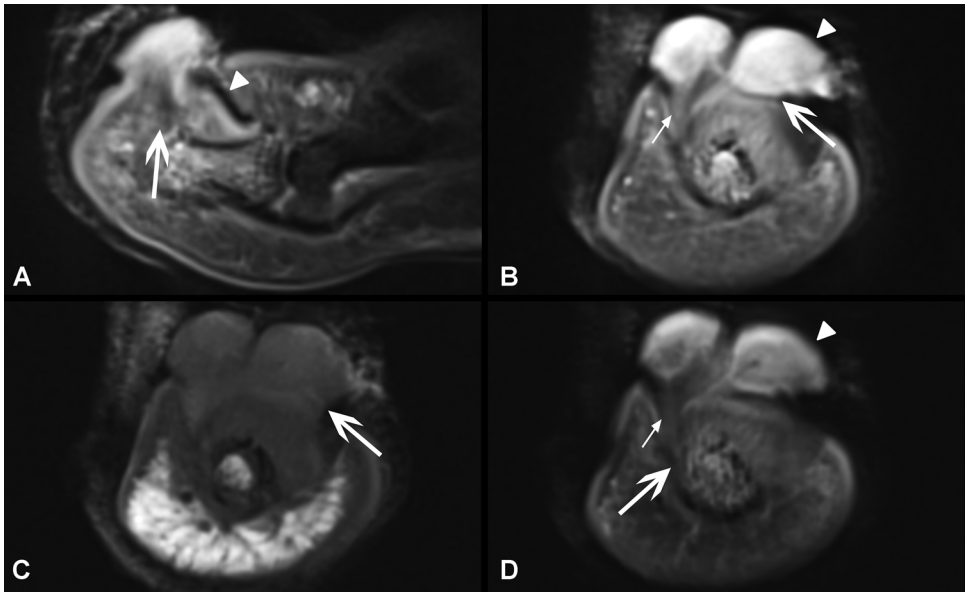

Fig. 4. Subungual keratoacanthoma. Lobulated mass arising from the distal part of the nail bed with mixed signal intensity on proton density fat saturated sagittal and axial images (A and B- open arrows), and hypointense signal on T1 (C- open arrow). Inflammatory changes and oedema around the tumor appear hyperintense on proton density (B- arrowhead) and there is lesion enhancement on post -contrast T1 weighted fat-saturated images (D- arrowhead). The central keratin plaque of the tumor has a hypo to intermediate signal intensity on proton density image (B- short arrow) and reveals no enhancement on post contrast T1-weighted fat-saturated image (D- short arrow). The tumor elevates the nail plate (A –arrowhead) and causes bone erosion (D –arrow).

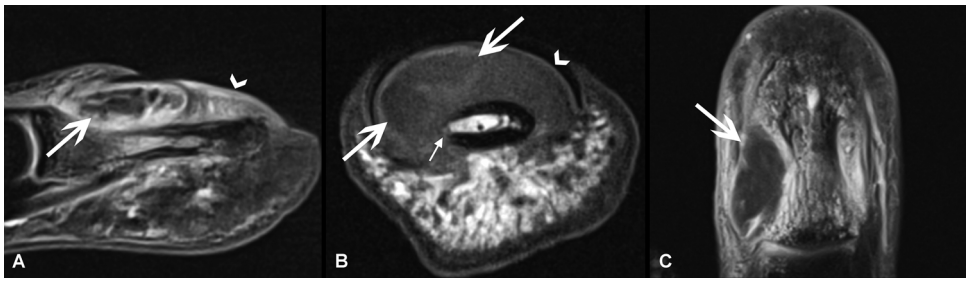

Fig. 5. Subungual fibroma arising from the proximal nail bed appears hypointense on proton density fat saturated sagittal images (A- arrow) and on T1-weighted axial (B- arrow). No enhancement on post contrast T1-weighted fat-saturated coronal image (C- arrow).

size [42]. Furthermore, the tumors were located on the palmar aspect of the distal phalanx. This study may have overestimated the positive predictive value of MRI due to a selection bias as all patients included in the study had a clinical diagnosis of glomus tumor before undergoing MRI [42]. Trehan et al. also demonstrated limited specificity and low negative predictive value of MRI in the diagnosis of glomus tumor of hands [43]. Both studies showed that although MRI was positive in all cases of subungual glomus tumors, in all false negative cases, the glomus tumors were not in subungual location, they had atypical histology or were too small (< 1–2 mm) to be detected by imaging.

Recurrence of glomus tumors as reported by various authors varies from 5% to 50% [37]. Theumann et all demonstrated that

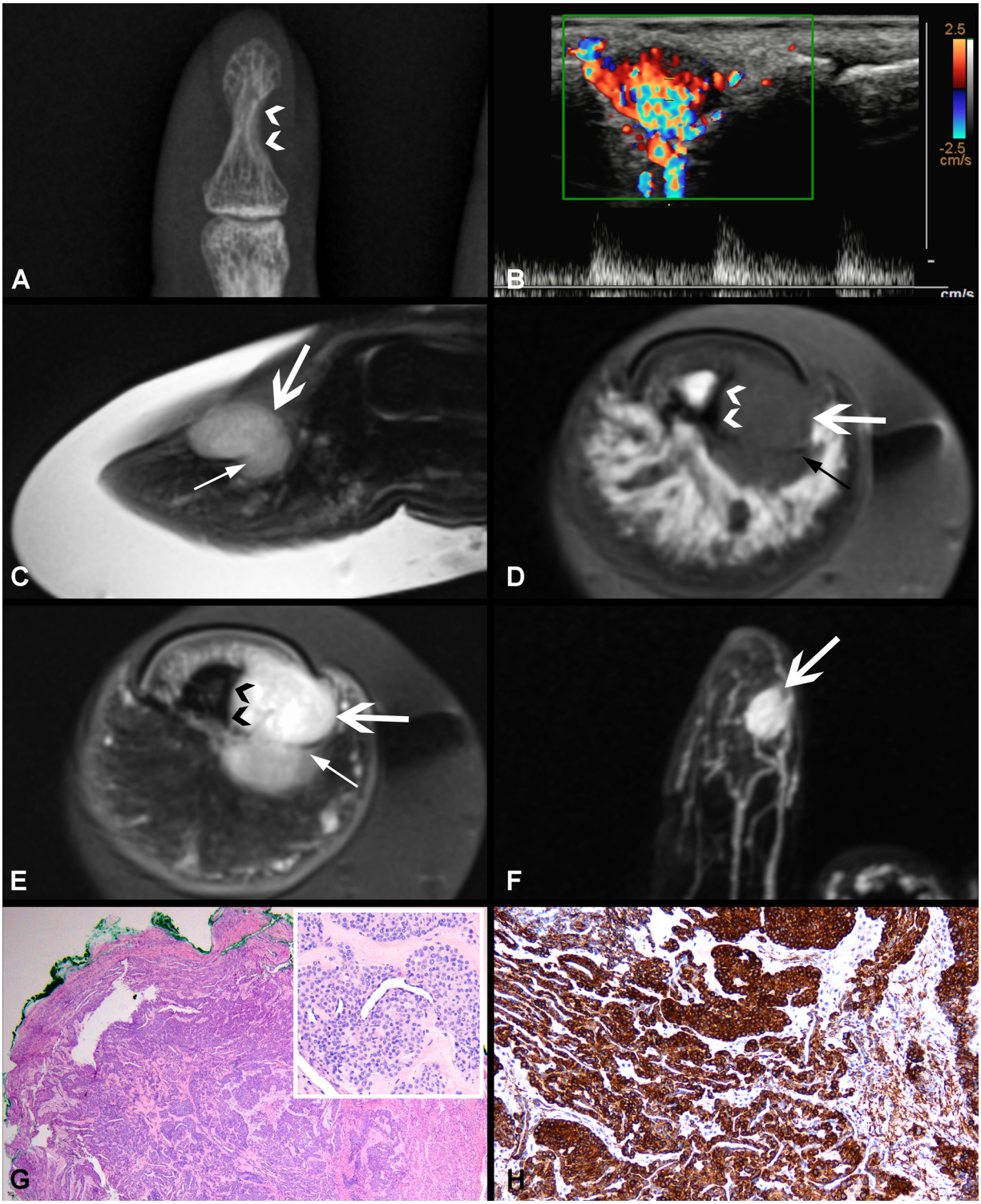

Fig. 6. Mixed type of glomus tumor. Anteroposterior radiograph of the index shows a regular bone erosion of the distal phalanx (A), confirmed on axial MR images (D and E- open arrowheads). High vascularity of the tumor detected by Doppler ultrasound (B) is correlated with intense enhancement in the arterial phase of MRI angiography (F- arrow). The lesion is mildly hyperintense on T2-weighted fat saturated sagittal image (C- open arrow), isointense to dermis on T1-weighted axial image (D- open arrow) and with strong enhancement on post contrast T1-weighted axial image (E- open arrow). Small arrows in C, D and E, point at tumor growth into the palmar side of the phalanx. The tumor is composed of small, uniform cells with a round central nucleus and pale eosinophilic cytoplasm, surrounding thin-walled vessels (G, Hematoxylin&Eosin, H&E, original magnification x20, inset x100). Glomus cells show strong and diffuse reactivity to smooth-muscle actin (H, x100), and to h-caldesmon *(not shown)*.

differentiation between scar tissue and recurrent glomus tumor was possible as many as 88% of cases [37]. Causes of recurrence include incomplete resection, missed diagnosis of coexisting second glomus tumor and development of new glomus tumor at the excision site. Theumann et al demonstrated the utility of MRI and MRI angiography for the diagnosis of recurrent glomus tumors [37]. Using 3D dynamic angiographic MRI sequences at 3 T, in our experience, the detection of smallest glomus tumors (< 2 mm) is greatly facilitated (Fig. 7).

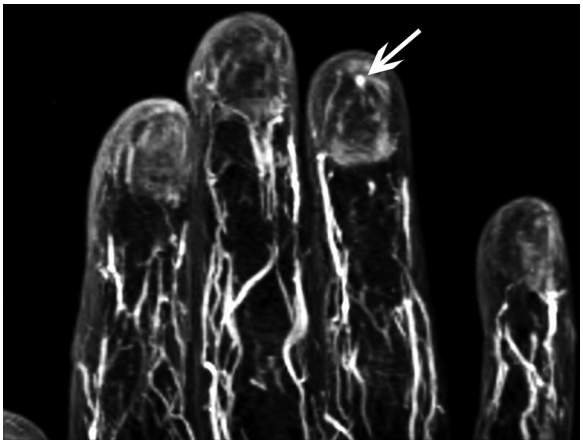

Fig. 7. Vascular type of glomus tumor less than 2 mm in size (white arrow) detected on a 3D TWIST (Time resolved angiography With Interleaved Stochastic Trajectories) MRI sequence.

Surgical techniques aimed at complete excision of glomus tumor include lateral subperiosteal approach, transungual approach with and without nail extraction, periungual approach and Mohs microsurgery. Location of the tumor in the nail apparatus determines the surgical approach in most instances. All techniques show more or less similar results [44–46] and pre-surgical tumor mapping is helpful for treatment planning.

5.5. Subungual exostosis

Subungual exostosis (Dupuytren exostosis) is a benign, solitary subungual bony tumor. It shows female preponderance and commonly occurs in adolescents and young adults. Commonest site of occurrence is the big toe. The exact etiology is unknown. Unlike osteochondroma, it reveals no cortical or marrow connectivity with the underlying bone. Pain and deformity are common symptoms. A plain radiograph is diagnostic and shows a non-aggressive bony outgrowth (Fig. 8). Ultrasound shows a hyperechoic mass with a hypoechoic fibrocartilagenous cap. The fibro-cartilaginous cap appears hyperintense on T2 weighted images (Fig. 8). Depending on its location and orientation, exostosis deforms the nail bed and matrix. These changes are best depicted on MRI. Symptomatic deformity of nail warrants surgical excision [4,5].

5.6. Hemangioma

Hemangioma is a superficial tumor, tending to develop in the superficial dermis and epidermis. Histologically, hemangioma is defined as a proliferation of vascular structures, lined by non-atypical endothelial cells. The lesion lacks the glomus cell component that characterizes glomus tumors [47]. At radiographic imaging, the presence of phebolits is characteristic. At US hemangioma appears hypoechoic, whereas – in the presence of fat – the lesion tends to be hyperechoic. Color Doppler US demonstrates vascular channels with a low resistance signal. Hemangioma shows intermediate signal on T1 weighted images and very high signal intensity on T2 weighted images. Reactive fat shows heterogeneous hyperintensity on T1 and T2 weighted images. The vascular component produces a serpentine pattern with flow void artifacts on T2 weighted images. Phlebolits produce low signal intensity on T1 and T2 weighted images. [5,48].

5.7. Pyogenic granuloma

Also known as lobular capillary hemangioma, pyogenic granuloma is a reactive lesion to trauma, infection, nerve injury or it may be induced by drugs (like retinoid, antiretroviral and chemotherapy agents). The lesion develops in the superficial soft tissues, predominantly in the fingers. Histologically, the lesion shows a characteristic lobular architecture and is composed of a vascular proliferation with varying inflammation and edema. The overlying epidermis is thinned and may show erosion or ulceration [49]. Clinically, pygogenic granuloma appears as a solitary red mass with frequent ulceration and bleeding. At US, the lesion presents as a well-defined mass with hyperechoic foci, this pattern allowing differentiation from hemangioma and glomus tumor. On Doppler, the tumor is hypervascular with arterial flow. On T1 weighted sequences, the lesion is isointense and it is hyperintense on T2. Marked enhancement is typically seen after injection of gadolinium chelates [5]. Treatment choice is done in accordance with the cause [50].

5.8. Chondroma

The fingers are the preferred location of chondromas (80% of cases) that, however, remain rare in the distal phalanx. According to Takigawa [52], only 4% of isolated chondroma and 13% of lesions arising in the setting of enchondromatosis are located in the third phalanx. The nail plate is very rarely involved [53]. Extra-skeletal chondroma has also been reported but is extremely rare [54]. Histologically, chondroma appears as a well-circumscribed lobulated mass of hyaline cartilage with variable cellularity and round nuclei. A rich interlobular connective tissue separates the lobules with large areas of fibrocartilaginous degeneration. The painful tumor may manifest with nail deformity, dystrophy or with nail fracture. On conventional X-rays, the mass is extra-osseous and contains typical calcifications in up to 70% of cases. On US, chondroma is hypoechoic and heterogeneous with marked hypervascularity on Doppler. It appears isointense on T1 weighted images, hyperintense on T2 weighted images and with strong enhancement after gadolinium injection. Foci of hypointenisty are frequently visible corresponding to calcifications.

6. Tumor-like lesions

6.1. Mucoid cyst

Mucoid cysts of the nail commonly occur at the proximal nail fold. Histopathologically, the mucoid cyst is a mucin filled space lined by fibroblasts. About 30% of mucoid cysts arise in the nail bed dermis and sub-matricial dermis and cause bone erosion and compression of the matrix [5,19,55]. The high incidence of post-surgical recurrence warrants imaging to depict the communication with the distal interphalangeal joint [5,55]. Sub-matricial mucoid cysts can be detected only on MRI [19]. MRI typically reveals a peduncle connecting the mucoid cyst with the inter-phalangeal joint along the lateral and inferior aspect of the extensor tendon insertion (Fig. 9). Multiloculated or unilocular satellite mucoid cysts seen in the peri-articular soft tissues with no relation to the interphalangeal joint most like represent myxomatous degeneration. Mucoid cysts appear T2-hyperinetense and show thin wall, and, occasionally septations. Post-gadolinium injection, fat saturated T1- weighted images show a thin enhancing wall on early phase and centripetal enhancement on delayed phase [55]. Surgical treatment includes excision of the cyst after identification and tying of the pedicle.

6.2. Epidermoid cyst

Epidermoid cyst is a benign lesion, clinically close to subungual tumor with bone involvement. It appears on histology as a benign cystic lesion lined by non-atypical squamous cells. On conventional X-rays, epidermoid cysts appear as expansile radiolucent osteolytic bone lesions, with cortical erosions involving the distal phalanx. On US, the lesion presents as a well-circumscribed mass with foci of hyperechogenecity and an « onion-ring appearance » due to the alternating

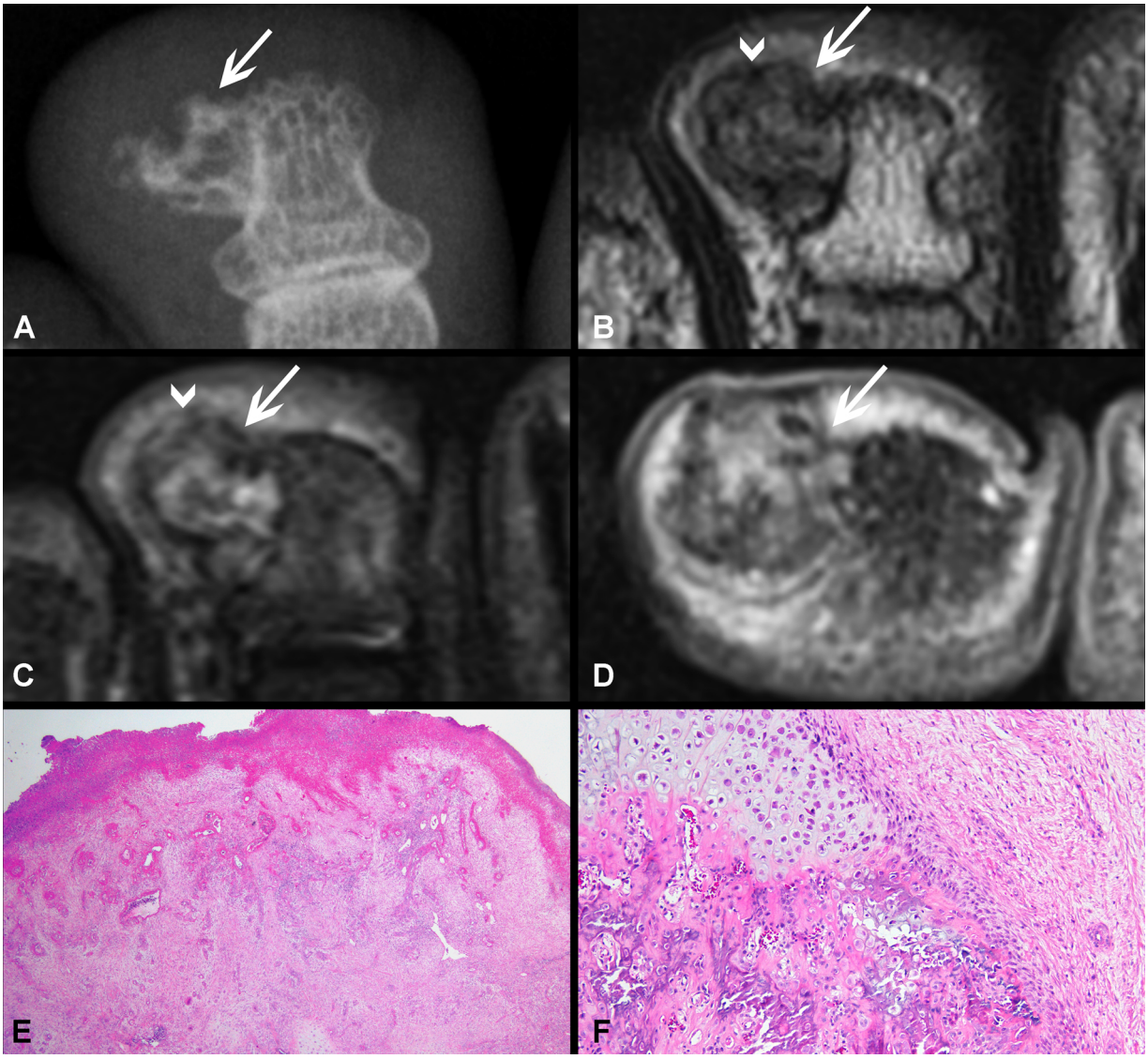

Fig. 8. Exostosis. Anteroposterior radiograph of great toe shows a characteristic bony protuberance arising from the distal phalanx without any continuation with the cortex and the medullary cavity of the phalanx (A- arrow). On coronal T2-weighted (B) and STIR (C) images, the tumor (B and C- arrow) and its fibro-cartilaginous cap (B and C- arrowheads) appear hypointense and hyperintense, respectively. Enhancement on post contrast T1-weighted fat-saturated axial image (D- arrow). At low magnification, superficial ulceration is seen, with a fibrin cap overlying a granulation tissue (E, H&E, x20). At higher magnification, the deeper portion of the lesion is composed of a peripheral spindle cell component, blending into hyaline cartilage and immature bone (F, H&E, x100).

hypoechoic and hyperechoic rings [51]. Color Doppler US confirms the absence of vascularity. On MRI, epidermoid cysts are iso or hyperintense on T1 and hyperintense on T2 weighted images; a thin peripheral rim enhancement after gadolinium injection is usually seen. T1 hyperintensity is caused by heterogeneous components, such as multiple layers of keratin. On diffusion weighted imaging, epidermoid cysts typically show restricted diffusivity. Although on conventional X ray and US, the differential diagnosis includes aneurysmal bone cyst and enchondroma, due to the characteristic restricted diffusivity on MRI, the diagnosis on the latter modality is straightforward. Curettage with bone grafting is performed in the majority of cases [5].

7. Malignant tumors

7.1. Squamous cell carcinoma of nail apparatus

Squamous cell carcinoma (SCC) of nail apparatus is a low-grade malignancy, which may occur at subungual and periungual locations. It affects finger more than toes, most commonly the thumb and index

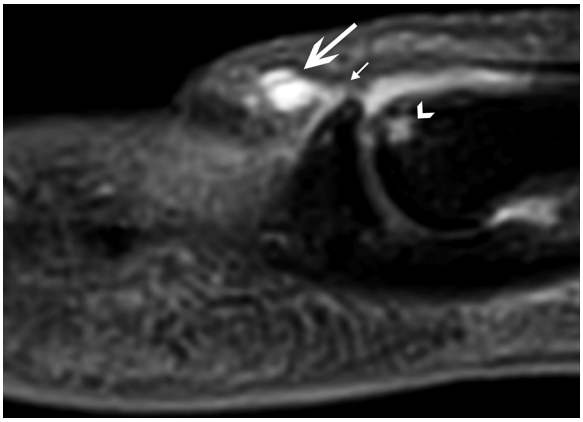

Fig. 9. Mucoid cyst in the proximal nail fold (open arrow), with fluid signal intensity on the T2-weighted fat-saturated sagittal image and with a thin communication with the proximal interphalangeal joint (small arrow). Osteoarthritic changes with subarticular geode are seen in the proximal interphalangeal joint (arrowhead).

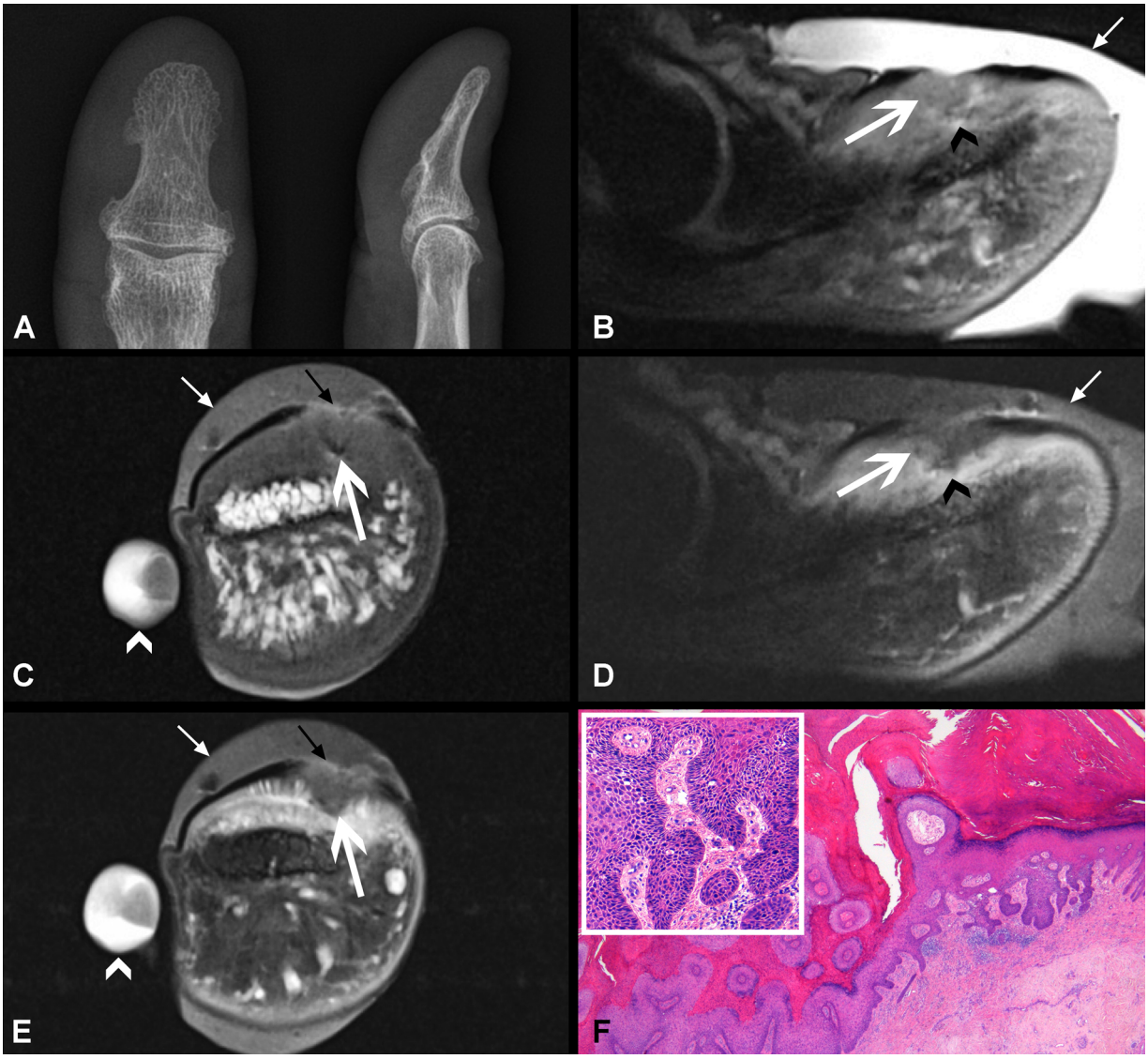

Fig. 10. Squamous cell carcinoma of the thumb. A patient treated with Mohs microsurgery for periungual SCC in situ, developed recurrent cancer, which is involving the nail bed (B, C, D and E- open arrows), the dermis (B and D- black arrowheads) and the nail plate (C and E- small black arrows). As compared to the dermis and normal nail bed, the recurrent mass appears isointense on T1-weighted axial image (C- open arrow), intermediate to hypointense on sagittal proton density images (B- open arrow) and appears hypo-enhancing on post- contrast T1-weighted fat-saturated sagittal and axial images (D and E- open arrows). No periosteal reaction or bone erosion is seen on MRI and plain radiography (A). Histology shows an atypical squamous cell proliferation, infiltrating the dermis F, H&E, 20x). Tumor cells show moderate to severe atypia (inset, x100). Overlying and adjacent epithelium shows hyperplastic papillomatous acanthosis, consistent with a viral papilloma. The tumor was positive for human papilloma virus type 16 (HPV16). This patient was treated with amputation of the distal phalanx. Small white arrows showing ultrasound gel on the skin in a glove (B–E). White arrowheads in C and E show skin marker on the medial aspect of the thumb.

finger, and involvement of multiple fingers or toes is rare. It shows male preponderance and the mean age of detection is 60 years. The exact etiology of ungual SCC is unknown. Nevertheless, genital digital human papilloma virus transmission (HPV type 16) is sighted as a cause of higher incidence in fingers than toes. Other predisposing factors reported in the literature include chronic paronychia, chronic repetitive trauma, congenital ectodermal dysplasia and prior radiation exposure. Various clinical presentations include painful and painless swelling, nail deformity and discoloration, purulent or bloody discharge, warty growth and ulceration. Obscuration by the nail plate precludes early detection of subungual SCC. The indolent clinical course of subungual SCC mimics other conditions including chronic fungal infection, warts, granuloma, periungual verrucae, glomus tumor, subungual keratoacanthoma, subungual fibroma and implantation dermoid cyst.

Histopathologically, ungual SCC is a malignancy of epithelial keratocytes. In situ SSC (Bowen`s disease) shows intact basal membrane whereas invasive SCC shows infiltration of the dermis. Thickened epithelium shows dyskeratotic cells, clumping of cells, scattered mitotic figures and necrotic keratocytes. Histopathological differential diagnosis includes subungual epidermoid cysts and keratoacanthoma [24].

The literature on the imaging features of nail apparatus SCC is sparse. Cramer et all described that plain radiography shows bony erosion with periosteal reaction and minimal sclerosis in long standing cases of subungual SCC [29]. On ultrasound, it appears as an irregularly marginated hypoechoic mass with internal vascularity [5]. On MRI, SCC shows ill-defined infiltrative margins, hypointense signal on T1 weighted images, intermediate to hyperintense signal on T2-weighted images, and enhancement on post-gadolinium fat saturated T1-weighted images (Fig. 10) [56–58]. On diffusion-weighted imaging, the tumor shows restricted diffusivity. Cortical erosion of the adjacent bone suggests tumor invasion. However, to differentiate the reactive periosteal reaction and marrow oedema pattern from tumor invasion on

Table 2
Summary of radiologic findings of nail tumors and tumor-like lesions.

Nail tumors and tumor-like lesions	Conventional X ray	Ultrasonography	High resolution MRI
Onychomatricoma	Non contributive	Avascular mass Hypoechoic and hyperechoic internal linear areas	Hyperintense, well-defined mass lesion, characteristic filamentous extensions on T2 Homogeneous lesion enhancement after injection of gadolinium.
Subungual keratoacanthoma	Mostly non contributive Occasionally cup shaped erosion of distal phalanx	Mixed echogenic avascular mass with posterior acoustic enhancement	Mass with intermediate signal intensity on T1 and mixed signal intensity on T2. Thin rim enhancement after injection of gadolinium.
Subungual fibroma	Non contributive or non-specific soft tissue swelling	Homogenous hypovascular mass	Most often low signal intensity on all sequences Mildly heterogeneous hyperintense appearance on T2 is correlated to the presence of mucoid stroma.
Glomus tumor	Occasionally bone erosion, intraosseous lytic lesion	Hypoechoic solid mass High-velocity flow on color Doppler	Vascular glomus: hyperintense on T2. MRI angiography: avid enhancement in the arterial phase, progressive enhancement in the venous phase. Solid glomus: isointense to dermis on pre- and post-gadolinium sequences. Thin hypointense capsule, bone erosion and matrix indentation on thin slice gradient echo 3D images. Mucoid glomus: hyperintense on T2 and rim enhancement.
Subungual exostosis	Characteristic bony outgrowth	Hyperechoic mass with a hypoechoic fibrocartilagenous cap	Deformation of the nail bed and matrix Fibro-cartilaginous portion hyperintense on T2.
Hemangioma	Occasionally phleboliths	Hypoechoic, if fat hyperechoic Low resistance vessels on color Doppler	Intermediate on T1, very high signal intensity on T2, heterogenous if fat, Flow void artifacts on T2 due to vascular component, phlebolits with low signal intensity on T1 and T2, progressive slow enhancement on dynamic MRI angiography sequences
Pygenic granuloma	Non contributive	Well-defined hyperechoic foci Hypervascular with arterial flow on Doppler	Isointense on T1, hyperintense on T2, intense enhancement after gadolinium injection
Chondroma	Often (70%) cartilaginous calcifications	Heterogeneous and hypoechoic Hypervascular on color Doppler	Isointense on T1, hyperintense on T2, strong enhancement after gadolinium injection, Foci of hypointenisty corresponding to calcifications.
Mucoid cyst	Non contributive in sub-matricial location	Non contributive in sub-matricial location	Peduncle connecting the mucoid cyst with the inter-phalangeal joint Multiloculated or unilocular pattern (myxomatous degeneration) T2 hyperinense, thin wall, occasionally septations. Thin enhancing wall on early phase and centripetal enhancement on delayed phase.
Epidermoid cyst	Non specific radiolucent bone lesion	Avascular well defined mass Usually characteristic alternating hypoechoic and hyperechoic rings	On T1, hypointense but occasionally hyperintense (layers of keratin), On T2, hyperintense Thin peripheral (rim) enhancement Characteristic restriction of diffusivity on diffusion weighted sequences
Squamous cell carcinoma of nail apparatus	Mostly non-contributive Bony erosion with periosteal reaction in long standing advanced tumors	Poorly delineated hypoechoic mass Non-specific internal vascularity	Ill-defined infiltrative margins, occasionally fluid filled necrotic areas in rapidly growing tumors. Hypointense on T1, intermediate to hyperintense on T2, enhancement after gadolinium injection. Restriction on diffusion weighted sequence. Cortical erosion suggests bone invasion. Marrow involvement seen as enhancement.
Malignant melanoma of nail apparatus	Nonspecific soft tissue swelling Occasionally bony erosion	Hypoechoic mass Highly vascular on color Doppler US allows measurement of tumor thickness (prognosis)	Signal intensity depends on melanin contents in the tumor: melanotic (hyperintense on T1, hypointense on T2), amelanotic or poorly melanotic (hypointense on T1, intermediate to hyperintense on T2) Strong enhancement after intravenous gadolinium. Precise measurement of size and thickness (prognosis)

imaging is difficult [5]. A reported case of rapidly grown subungual SCC showed fluid filled necrotic areas [58]. Lymph node metastasis is extremely rare (less than 2%) in subungual SCC [59].

The choice of the surgical method for subungual SCC depends on the presence or absence of bony invasion. In the absence of bony invasion, commonly used surgical methods include local excision, wide excision and Mohs microsurgery. Use of distal phalangeal amputation and complete digital amputation depend on the extent of bone involvement. Some authors propose a combination of radiation therapy and Mohs microsurgery [13,59–61].

7.2. Malignant melanoma of nail apparatus

Melanoma of nail apparatus includes that of subungual, ungual and periungual regions. Acral lentiginous type of malignant melanoma commonly occurs in nail apparatus. Fingernails are more affected than toenails, and the commonest locations are thumb and great toe [62]. It shows peak incidence in the 5th-7th decade and no gender preponderance. The exact pathogenesis of the subungual melanoma is uncertain. Few authors consider previous trauma as a possible cause [62]. Clinical presentation includes nail dystrophy, pigmentation of nail and periungual soft tissue, split nail, chronic painful swelling, ingrown nail, pigmented nail streak, and junctional nevus. Amelanotic melanoma presents as red nodule extruding through nail plate [5,62,63].

Subungual melanoma carries a poor prognosis as compared to melanoma at other locations. Factors responsible for its poor prognosis include the delay in the initial diagnosis, its rapid horizontal growth pattern and tendency to metastasize early. Several factors contribute to

the delay in the diagnosis of subungual melanoma, which includes non-specific clinical presentation, the frequent occurrence of amelanotic melanoma in this location and, also, the anatomical context of the nail apparatus, which makes early diagnosis difficult [63]. Histopathological findings of subungual melanoma include prominent lentiginous growth with single cells showing moderate to severe atypia, and dense pagetoid spread. Other findings include atypical melanocytes, acanthosis and rete ridges.

Plain radiography findings in subungual melanoma comprise non-specific soft tissue swelling and, sometimes, bony erosion. On ultrasound, it appears as a solid, hypoechoic and highly vascular mass. Measurement of tumor thickness on ultrasound helps in determining the prognostic outcome of cutaneous melanoma, and it correlates with histological assessment of tumor [64]. Evaluation of angiogenesis and neovascularity on US Doppler predicts the metastatic potential of malignant melanoma [65]. As the above-mentioned ultrasound studies evaluated cutaneous melanomas, the reproducibility of these results in subungual malignant melanoma remains undetermined.

MRI appearance of subungual malignant melanoma depends on the melanin contents in the tumor. Melanotic malignant melanoma of subungual space appears hyperintense on T1 weighted and hypointense on T2 weighted images. In contrast, amelanotic melanoma or melanoma with low melanin content appears hypointense on T1 and intermediate to hyperintense on T2 weighted images. Presence of hemorrhage also influences the MRI appearance of melanoma. High-resolution MRI allows precise lesion measurement, in particular the estimation of tumor thickness.

Preferred surgical treatment for non-invasive and in situ subungual melanoma includes wide excision up to periosteum and Mohs microsurgery. Amputation at the nearest uninvolved joint is preferred for invasive subungual melanomas.

8. Summary

In this article, we explain and illustrate the state-of-the-art MRI protocol at 3 T and describe the clinical, histologic and imaging characteristics of common nail tumors and tumor-like lesions. Emphasis is put on characteristic MRI findings. Although MRI features are not entirely specific, the high sensitivity of MRI for lesion detection and for precise depiction of patterns of deep tumor spread make it a valuable tool for treatment planning.

References

[1] C. Soligo, A.E. Muller, Nails and claws in primate evolution, J. Hum. Evol. 36 (1) (1999) 97–114.
[2] P.R. Cohen, Metastatic tumors to the nail unit: subungual metastases, Dermatol. Surg. 27 (3) (2001) 280–293.
[3] J.L. Drape, Imaging of tumors of the nail unit, Clin. Podiatr. Med. Surg. 21 (4) (2004) 493–511.
[4] J.L. Drape, Imaging of the tumors of the perionychium, Hand Clin. 18 (4) (2002) 655–670 discussion 671.
[5] H.J. Baek, S.J. Lee, K.H. Cho, H.J. Choo, S.M. Lee, Y.H. Lee, K.J. Suh, T.Y. Moon, J.G. Cha, J.H. Yi, M.H. Kim, S.J. Jung, J.H. Choi, Subungual tumors: clinicopathologic correlation with US and MR imaging findings, Radiographics 30 (6) (2010) 1621–1636.
[6] E.G. Zook, Anatomy and physiology of the perionychium, Clin. Anat. (New York, N.Y.) 16 (1) (2003) 1–8.
[7] D. Berritto, F. Iacobellis, C. Rossi, A. Reginelli, S. Cappabianca, R. Grassi, Ultra high-frequency ultrasound: new capabilities for nail anatomy exploration, J. Dermatol. 44 (1) (2017) 43–46.
[8] J.L. Drape, W. Wolfram-Gabel, I. Idy-Peretti, R. Baran, S. Goettmann, H. Sick, H. Guerin-Surville, J. Bittoun, The lunula: a magnetic resonance imagining approach to the subnail matrix area, J. Invest. Dermatol. 106 (5) (1996) 1081–1085.
[9] D. McGonagle, Enthesitis: an autoinflammatory lesion linking nail and joint involvement in psoriatic disease, J. Eur. Acad. Dermatol. Venereol. 23 (Suppl. 1) (2009) 9–13.
[10] D. McGonagle, A.L. Tan, M. Benjamin, The nail as a musculoskeletal appendage–implications for an improved understanding of the link between psoriasis and arthritis, Dermatology (Basel, Switzerland) 218 (2) (2009) 97–102.
[11] J.L. Drape, I. Idy-Peretti, S. Goettmann, H. Guerin-Surville, J. Bittoun, Standard and high resolution magnetic resonance imaging of glomus tumors of toes and fingertips, J. Am. Acad. Dermatol. 35 (4) (1996) 550–555.
[12] F. Gandon, P. Legaillard, R. Brueton, D. Le Viet, G. Foucher, Forty-eight glomus tumours of the hand. Retrospective study and four-year follow-up, Annales de chirurgie de la main et du membre superieur: organe officiel des societes de chirurgie de la main = Annals of hand and upper limb surgery 11 (5) (1992) 401–405.
[13] S.R. Peterson, E.G. Layton, A.K. Joseph, Squamous cell carcinoma of the nail unit with evidence of bony involvement: a multidisciplinary approach to resection and reconstruction, Dermatol. Surg. 30 (2 Pt 1) (2004) 218–221.
[14] X. Wortsman, J. Wortsman, R. Soto, T. Saavedra, J. Honeyman, I. Sazunic, Y. Corredoira, Benign tumors and pseudotumors of the nail: a novel application of sonography, J. Ultrasound Med. 29 (5) (2010) 803–816.
[15] F. Aluja, D.C. Jaramillo, Quiasua Mejia, H.M. Martinez Orduz, C. Gonzalez Ardila, Nail unit ultrasound: a complete guide of the nail diseases, J. Ultrasound 20 (3) (2017) 181–192.
[16] B.D. Fornage, Glomus tumors in the fingers: diagnosis with US, Radiology 167 (1) (1988) 183–185.
[17] B.D. Fornage, F.L. Schernberg, M.D. Rifkin, D.H. Touche, Sonographic diagnosis of glomus tumor of the finger, J. Ultrasound Med. 3 (11) (1984) 523–524.
[18] X. Wortsman, G.B. Jemec, Role of high-variable frequency ultrasound in preoperative diagnosis of glomus tumors: a pilot study, Am. J. Clin. Dermatol. 10 (1) (2009) 23–27.
[19] B. Richert, M. Baghale, Medical imaging and MRI in nail disorders: report of 119 cases and review of the literature, Dermatol. Ther. 15 (2) (2002) 159–164.
[20] R. Baran, A. Kint, Onychomatrixoma. Filamentous tufted tumour in the matrix of a funnel-shaped nail: a new entity (report of three cases), Br. J. Dermatol. 126 (5) (1992) 510–515.
[21] K.J. Willard, M.A. Cappel, S.H. Kozin, J.M. Abzug, Benign subungual tumors, J. Hand Surg. 37 (6) (2012) 1276–1286 quiz 1286.
[22] E.M. Gaertner, M. Gordon, T. Reed, Onychomatricoma: case report of an unusual subungual tumor with literature review, J. Cutan. Pathol. 36 (Suppl. 1) (2009) 66–69.
[23] N. Spaccarelli, K.A. Wanat, C.J. Miller, A.I. Rubin, Hypopigmented onychocytic matricoma as a clinical mimic of onychomatricoma: clinical, intraoperative and histopathologic correlations, J. Cutan. Pathol. 40 (6) (2013) 591–594.
[24] J. Andre, U. Sass, B. Richert, A. Theunis, Nail pathology, Clin. Dermatol. 31 (5) (2013) 526–539.
[25] E. Cinotti, G. Veronesi, B. Labeille, F. Cambazard, B.M. Piraccini, E. Dika, J.L. Perrot, P. Rubegni, Imaging technique for the diagnosis of onychomatricoma, J. Eur. Acad. Dermatol. Venereol. 32 (11) (2018) 1874–1878.
[26] M.S. Graves, J.K. Anderson, K.G. LeBlanc Jr., D.J. Sheehan, Utilization of Mohs micrographic surgery in a patient with onychomatricoma, Dermatol. Surg. 41 (6) (2015) 753–755.
[27] J.H. Choi, D.H. Shin, D.S. Shin, K.H. Cho, Subungual keratoacanthoma: ultrasound and magnetic resonance imaging findings, Skeletal Radiol. 36 (8) (2007) 769–772.
[28] A. Sinha, R. Marsh, J. Langtry, Spontaneous regression of subungual keratoacanthoma with reossification of underlying distal lytic phalynx, Clin. Exp. Dermatol. 30 (1) (2005) 20–22.
[29] S.F. Cramer, Subungual keratoacanthoma. A benign bone-eroding neoplasm of the distal phalanx, Am. J. Clin. Pathol. 75 (3) (1981) 425–429.
[30] R. Minotto, L. Dalla Corte, A.L. Boff, M. Vale Scribel de Silva, M. Resener de Morais, Subungual keratoacanthoma: a case report, Surg Cosmet Dermatol 6 (4) (2014) 377–379.
[31] V.D. Pellegrini Jr., A. Tompkins, Management of subungual keratoacanthoma, J. Hand Surg. 11 (5) (1986) 718–724.
[32] R. Baran, G. Mikhail, B. Costini, A. Tosti, S. Goettmann-Bonvallot, Distal digital keratoacanthoma: two cases with a review of the literature, Dermatol. Surg. 27 (6) (2001) 575–579.
[33] T. Kojima, T. Nagano, M. Uchida, Periungual fibroma, J. Hand Surg. 12 (3) (1987) 465–470.
[34] T. Moriue, K. Yoneda, J. Moriue, K. Nakai, Y. Kubota, Multibranched acquired periungual fibrokeratoma, JAMA Dermatol. 150 (4) (2014) 456–457.
[35] R.E. Carroll, A.T. Berman, Glomus tumors of the hand: review of the literature and report on twenty-eight cases, J. Bone Joint Surg. Am. 54 (4) (1972) 691–703.
[36] M. Mravic, G. LaChaud, A. Nguyen, M.A. Scott, S.M. Dry, A.W. James, Clinical and histopathological diagnosis of glomus tumor: an institutional experience of 138 cases, Int. J. Surg. Pathol. 23 (3) (2015) 181–188.
[37] N.H. Theumann, S. Goettmann, D. Le Viet, D. Resnick, C.B. Chung, J. Bittoun, A. Chevrot, J.L. Drape, Recurrent glomus tumors of fingertips: MR imaging evaluation, Radiology 223 (1) (2002) 143–151.
[38] B. Harrison, A.M. Moore, R. Calfee, D.M. Sammer, The association between glomus tumors and neurofibromatosis, J. Hand Surg. 38 (8) (2013) 1571–1574.
[39] K.W. Ham, I.S. Yun, K.C. Tark, Glomus tumors: symptom variations and magnetic resonance imaging for diagnosis, Arch. Plast. Surg. 40 (4) (2013) 392–396.
[40] S.H. Chen, Y.L. Chen, M.H. Cheng, K.M. Yeow, H.C. Chen, F.C. Wei, The use of ultrasonography in preoperative localization of digital glomus tumors, Plast. Reconstr. Surg. 112 (1) (2003) 115–119 discussion 120..
[41] Y.P. Chiang, C.Y. Hsu, W.C. Lien, Y.J. Chang, Ultrasonographic appearance of subungual glomus tumors, J. Clin. Ultrasound 42 (6) (2014) 336–340.
[42] M.M. Al-Qattan, A. Al-Namla, A. Al-Thunayan, F. Al-Subhi, A.F. El-Shayeb, Magnetic resonance imaging in the diagnosis of glomus tumours of the hand, J. Hand Surg. (Edinburgh, Scotland) 30 (5) (2005) 535–540.
[43] S.K. Trehan, E.A. Athanasian, E.F. DiCarlo, D.N. Mintz, A. Daluiski, Characteristics of glomus tumors in the hand not diagnosed on magnetic resonance imaging, J. Hand Surg. 40 (3) (2015) 542–545.
[44] T.L. Roan, C.K. Chen, S.Y. Horng, J.H. Hsieh, H.C. Tai, M.H. Hsieh, H.F. Chien, Y.B. Tang, Surgical technique innovation for the excision of subungual glomus

tumors, Dermatol. Surg. 37 (2) (2011) 259–262.
[45] S.S. Cernea, N. Di Chiacchio, A. Vanti, Subungueal glomus tumors treated by the mohs micrographic surgery: recurrence index and literature review, Surg. Cosmet. Dermatol. 1 (2) (2009) 70–73.
[46] B. Garg, M.V. Machhindra, V. Tiwari, V. Shankar, P. Kotwal, Nail-preserving modified lateral subperiosteal approach for subungual glomus tumour: a novel surgical approach, Musculoskelet. Surg. 100 (1) (2016) 43–48.
[47] P.W. Allen, F.M. Enzinger, Hemangioma of skeletal muscle. An analysis of 89 cases, Cancer 29 (1) (1972) 8–22.
[48] N.H. Theumann, J. Bittoun, S. Goettmann, D. Le Viet, A. Chevrot, J.L. Drape, Hemangiomas of the fingers: MR imaging evaluation, Radiology 218 (3) (2001) 841–847.
[49] B.M. Piraccini, S. Bellavista, C. Misciali, A. Tosti, D. de Berker, B. Richert, Periungual and subungual pyogenic granuloma, Br. J. Dermatol. 163 (5) (2010) 941–953.
[50] B. Richert, P. Lecerf, M. Caucanas, J. Andre, Nail tumors, Clin. Dermatol. 31 (5) (2013) 602–617.
[51] A. Arora, D. Srivastava, H. Gupta, V. Kumar, P.P. Kotwal, Sonographic diagnosis of subungual intraosseous epidermoid cyst, J. Clin. Ultrasound 41 (Suppl 1) (2013) 35–37.
[52] K. Takigawa, Chondroma of the bones of the hand. A review of 110 cases, J. Bone Jt. Surg. 53 (8) (1971) 1591–1600. American.
[53] C.A. Dumontier, P. Abimelec, Nail unit enchondromas and osteochondromas: a surgical approach, Dermatol. Surg. 27 (3) (2001) 274–279.
[54] T. Ishii, M. Ikeda, Y. Oka, Subungual extraskeletal chondroma with finger nail deformity: case report, J. Hand Surg. 35 (2) (2010) 296–299.
[55] J.L. Drape, I. Idy-Peretti, S. Goettmann, A. Salon, P. Abimelec, H. Guerin-Surville, J. Bittoun, MR imaging of digital mucoid cysts, Radiology 200 (2) (1996) 531–536.
[56] S.J. Theodorou, D.J. Theodorou, S.J. Bona, S. Farooki, Primary squamous cell carcinoma: an incidental toe mass, Am. J. Roentgenol. 184 (Suppl. 3) (2005) S110–1.
[57] E. Inkaya, E. Sayit, A.T. Sayit, E. Zan, M. Bakirtas, Subungual squamous cell carcinoma of the third finger with radiologic and histopathologic findings: a report of case, J. Hand Microsurg. 7 (1) (2015) 194–198.
[58] H. Choughri, F. Villani, E. Sawaya, P. Pelissier, Atypical squamous cell carcinoma of the nail bed with phalangeal involvement, J. Plast. Surg. Hand Surg. 45 (3) (2011) 173–176.
[59] M.N. Zaiac, E. Weiss, Mohs micrographic surgery of the nail unit and squamous cell carcinoma, Dermatol. Surg. 27 (3) (2001) 246–251.
[60] P. Lecerf, B. Richert, A. Theunis, J. Andre, A retrospective study of squamous cell carcinoma of the nail unit diagnosed in a Belgian general hospital over a 15-year period, J. Am. Acad. Dermatol. 69 (2) (2013) 253–261.
[61] S. Dalle, L. Depape, A. Phan, B. Balme, S. Ronger-Savle, L. Thomas, Squamous cell carcinoma of the nail apparatus: clinicopathological study of 35 cases, Br. J. Dermatol. 156 (5) (2007) 871–874.
[62] A. Phan, S. Touzet, S. Dalle, S. Ronger-Savle, B. Balme, L. Thomas, Acral lentiginous melanoma: a clinicoprognostic study of 126 cases, Br. J. Dermatol. 155 (3) (2006) 561–569.
[63] E.K. Levit, M.H. Kagen, R.K. Scher, M. Grossman, E. Altman, The ABC rule for clinical detection of subungual melanoma, J. Am. Acad. Dermatol. 42 (2 Pt 1) (2000) 269–274.
[64] R. Vilana, S. Puig, M. Sanchez, M. Squarcia, A. Lopez, T. Castel, J. Malvehy, Preoperative assessment of cutaneous melanoma thickness using 10-MHz sonography, Am. J. Roentgenol. 193 (3) (2009) 639–643.
[65] N. Lassau, S. Koscielny, M.F. Avril, A. Margulis, P. Duvillard, T. De Baere, A. Roche, J. Leclere, Prognostic value of angiogenesis evaluated with high-frequency and color Doppler sonography for preoperative assessment of melanomas, Am. J. Roentgenol. 178 (6) (2002) 1547–1551.